Metal−Metal Bonding in $M_2Cl_6(H_2PCH_2PH_2)_2$, $M_2Cl_6(PH_3)_4$, and $M_2Cl_{10}^{4-}$ (M = Cr, Mo, W) Edge-Shared Dimer Systems

Robert Stranger,*,† Timothy Lovell,†,§ and John E. McGrady‡

Department of Chemistry, The Faculties, The Australian National University, Canberra, ACT 0200, Australia, and Department of Chemistry, The University of York, Heslington, York YO10 5DD, U.K.

Received May 10, 1999

Density functional theory is used to determine the electronic structures, geometries, and periodic trends in metal−metal bonding in the homo- and heterobimetallic d^3d^3 edge-shared systems $M_2Cl_{10}^{4-}$, $M_2Cl_6(PH_3)_4$, and $M_2Cl_6(H_2PCH_2PH_2)_2$ (M = Cr, Mo, W). The much shorter metal−metal distances in these complexes relative to $M_2Cl_{10}^{4-}$ (M = Mo, W) are shown to arise solely from electronic differences between chlorine and phosphine donors. Due to inversion of the δ and δ^* orbitals, the complexes $M_2Cl_6(PH_3)_4$ and $M_2Cl_6(H_2PCH_2PH_2)_2$ (M = Mo, W) are found to possess formal metal−metal double bonds. The periodic trends in metal−metal bonding in these systems are rationalized in terms of the energetic contributions of orbital overlap (ΔE_{ovlp}) and spin polarization (ΔE_{spe}). The reduction in ΔE_{spe} and increase in ΔE_{ovlp} on replacement of axial chlorides with phosphine both favor stronger metal−metal bonding in the phosphine-based complexes. The strong linear dependence observed between ΔE_{spe} and ΔE_{ovlp} enables the metal−metal bonding in these systems to be predicted simply from single-ion spin-polarization energies. The antiferromagnetic coupling in $M_2Cl_6(H_2PCH_2PH_2)_2$ (M = Mo, W) and $MoWCl_6(H_2PCH_2PH_2)_2$ is shown to be mostly due to coupling of the metal δ electrons, with a smaller contribution from the π electrons, particularly for the dimolybdenum complex.

Introduction

To address periodic trends in metal−metal bonding theoretically, the chosen methodology must be able to adequately describe all possible metal−metal interactions ranging from weak magnetic coupling through to multiple metal−metal bonding. In this regard, our earlier work focusing on d^3d^3 face-shared bioctahedral $M_2X_9^{3-}$ (M = Cr, Mo, W) dimers[1] showed that the broken-symmetry methodology of Noodleman and co-workers,[2] when incorporated into density functional based geometry optimization routines, was capable of reproducing the observed structural and magnetic trends in these systems ranging from strong metal−metal bonding in $W_2Cl_9^{3-}$ to weak antiferromagnetic coupling in $Cr_2Cl_9^{3-}$. Other workers have shown that the same methodology is also applicable in the study of internal rotation in quadruply metal−metal bonded dimers.[3]

More recently, we examined in detail the potential energy curves for the broken-symmetry and low-lying spin states in the d^3d^3 edge-shared decahalide system $M_2Cl_{10}^{4-}$ (M = Cr, Mo, W),[4] allowing a straightforward comparison of metal−metal bonding with the d^3d^3 face-shared $M_2Cl_9^{3-}$ dimers previously investigated. Although structural and magnetic data for the edge-shared decahalides $M_2Cl_{10}^{4-}$ are scarce, considerable data exist for the closely related edge-shared phosphine-bridged $M_2Cl_6(dmpm)_2$ and $M_2Cl_6(dppm)_2$ systems (dmpm = dimethylphosphinomethane; dppm = diphenylphosphinomethane).[5] Like their face-shared counterparts, significant variation in the metal−metal interactions is observed ranging from strong metal−metal bonding in $W_2Cl_6(dmpm)_2$ and $W_2Cl_6(dppm)_2$ to only weak magnetic coupling in the chromium analogues. These phosphine-bridged complexes provide an ideal opportunity not only to test the ability of current theoretical methods to reproduce structural data but also to examine periodic trends in metal−metal bonding. Therefore, our purpose in this paper is to extend our earlier analysis of the edge-shared decahalides to the edge-shared phosphine-bridged dimers $M_2Cl_6(H_2PCH_2PH_2)_2$ (M = Cr, Mo, W), which serve as a model system for the geometric and electronic structures of $M_2Cl_6(dmpm)_2$ and $M_2Cl_6(dppm)_2$ complexes. In doing so we aim to delineate the factors responsible for the variation in structural and magnetic properties of these systems through a systematic study of the electronic structure and metal−metal bonding in homobimetallic and heterobimetallic $M_2Cl_{10}^{4-}$, $M_2Cl_6(PH_3)_4$, and $M_2Cl_6(H_2PCH_2PH_2)_2$ (M = Cr, Mo, W) complexes (Chart 1).

Computational Details

All calculations described in this work were performed on either Sun UltraSparc 140/170 workstations or Linux-based Pentium II 333/400 MHz computers using the Amsterdam Density Functional (ADF) program, version 2.3, developed by Baerends et al.[6] The local density

† The Australian National University.

§ Current address: Department of Molecular Biology, The Scripps Research Institute, La Jolla, CA 92037.

‡ The Uversity of York.

(1) (a) Lovell, T.; McGrady, J. E.; Stranger, R.; Macgregor, S. A. *Inorg. Chem.* **1996**, *35*, 3079. (b) McGrady, J. E.; Stranger, R.; Lovell, T. *J. Phys. Chem. A* **1997**, *101* (1), 6265. (c) McGrady, J. E.; Stranger, R.; Lovell, T. *Inorg. Chem.* **1997**, *36*, 3242.

(2) (a) Noodleman, L.; Norman, J. G., Jr. *J. Chem. Phys.* **1979**, *70*, 4903. (b) Noodleman, L. *J. Chem. Phys.* **1981**, *74*, 5737. (c) Noodleman, L.; Case, D. A. *Adv. Inorg. Chem.* **1992**, *38*, 423.

(3) Lledos, A.; Jean, Y. *Inorg. Chem.* **1998**, *37*, 3321.

(4) McGrady, J. E.; Stranger, R.; Lovell, T. *Inorg. Chem.* **1998**, *37*, 3802.

(5) (a) Cotton, F. A.; Diebold, M. P.; O'Connor, C. J.; Powell, G. L. *J. Am. Chem. Soc.* **1985**, *107*, 7438. (b) Chakravarty, A. R.; Cotton, F. A.; Diebold, M. P.; Lewis, D. B.; Roth, W. J. *J. Am. Chem. Soc.* **1986**, *108*, 971. (c) Canich, J. M.; Cotton, F. A.; Daniels, L. M.; Lewis, D. B. *Inorg. Chem.* **1987**, *26*, 4046. (d) Cotton, F. A. *Polyhedron* **1987**, *6*, 667. (e) Cotton, F. A.; Eglin, J. L.; Luck, R. L.; Son, K.-A. *Inorg. Chem.* **1990**, *29*, 1802. (f) Poli, R.; Mui, H. D. *Inorg. Chem.* **1991**, *30*, 65. (g) Poli, R.; Gordon, J. C. *J. Am. Chem. Soc.* **1992**, *114*, 6723. (h) Cotton, F. A.; Eglin, J. L.; James, C. A.; Luck, R. L. *Inorg. Chem.* **1992**, *31*, 5308.

10.1021/ic9905042 CCC: $18.00 © 1999 American Chemical Society
Published on Web 11/09/1999

Chart 1

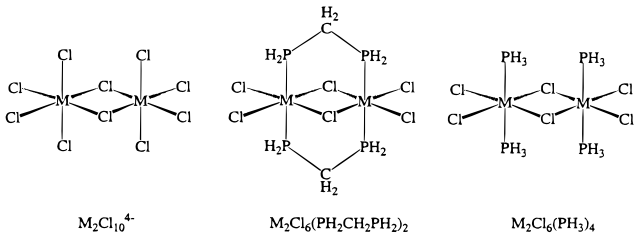

approximation to the exchange potential was used, along with the correlation potential of Vosko, Wilk, and Nusair.[7] The LDA was used throughout as previous work[1b] has shown that incorporation of nonlocal corrections to the exchange-correlation potential leads to generally poorer agreement with experiment, particularly in relation to metal−metal distances. A double-ζ Slater type orbital basis set extended with a single d-polarization function was used to describe the main group atoms, while all metals were modeled with triple-ζ basis sets. Electrons in orbitals up to and including 1s {C}, 2p {P}, 2p {Cl}, 3p {Cr}, 4p {Mo,}, and 5p {W} were considered to be part of the core and treated in accordance with the frozen-core approximation. Geometries were fully optimized using the algorithm of Versluis and Ziegler.[8] Full-symmetry calculations for the $S = 0-3$ associated states were performed in a spin-unrestricted manner using D_{2h} (homobimetallic) or C_{2v} (heterobimetallic) symmetry. In the broken-symmetry calculations, all symmetry elements connecting the two metal centers were removed, resulting in overall C_{2v} point group symmetry, and an asymmetry in the initial spin density introduced using the "modifystartpotential" key. Potential energy curves for the broken-symmetry and associated states were generated by freezing the metal−metal separation and optimizing all other structural parameters independently. Exchange coupling coefficients were calculated from the differences in energy (ΔSCF method) between the broken-symmetry state and its associated ferromagnetic counterpart using optimized geometries for both states.

Results and Discussion

Orbital Interactions. The general features of the interaction involving the metal-based orbitals in $M_2Cl_{10}^{4-}$, $M_2Cl_6(PH_3)_4$, and $M_2Cl_6(H_2PCH_2PH_2)_2$ systems are shown in Figure 1. From a group theoretical analysis, the local C_{2v} symmetry at each metal center splits the degenerate t_{2g} orbitals into nondegenerate $a_1 + b_2 + a_2$ levels having σ, π, and δ symmetry with respect to the metal−metal axis. In the weakly coupled (localized) limit, these magnetic orbitals remain essentially localized on the metal centers and, in the case of d^3d^3 dimers, are singly occupied. Metal−metal orbital overlap results in delocalization of the magnetic orbitals over both metal centers and consequent formation of metal−metal bonding $a_g(\sigma)$, $b_{2u}(\pi)$, and $b_{1g}(\delta)$ and antibonding $b_{1u}(\sigma^*)$, $b_{3g}(\pi^*)$, and $a_u(\delta^*)$ molecular orbitals. The splittings within the energy levels shown in Figure 1 arise from two very different sources. In the weakly coupled limit spin polarization is responsible for the separation of the occupied and vacant single-ion orbitals, whereas in the delocalized limit, metal−metal orbital overlap causes splitting between bonding and antibonding molecular orbitals. The position of the localized/delocalized equilibrium in these complexes, and therefore the resulting geometries and extent of metal−metal bonding, will depend on the relative magnitudes of these two factors.

Optimized Geometries. The relevant broken-symmetry (C_{2v}) optimized structural parameters for $M_2Cl_{10}^{4-}$, $M_2Cl_6(PH_3)_4$, and $M_2Cl_6(H_2PCH_2PH_2)_2$ (M = Cr, Mo, W) complexes are summarized in Table 1, the available experimental data for $M_2Cl_6(dmpm)_2$ and $M_2Cl_6(dppm)_2$ systems are given in Table 2. It should be noted that because of crystallographic disorder, the values given in Table 2 for $MoWCl_6(dmpm)_2$ and $MoWCl_6(dppm)_2$ are averaged over both metal centers. On the whole, the calculated geometries are in reasonable agreement with the crystallographic data. In general, smaller metal−ligand bond distances are calculated in line with the known tendency of the LDA to underestimate these distances.[9]

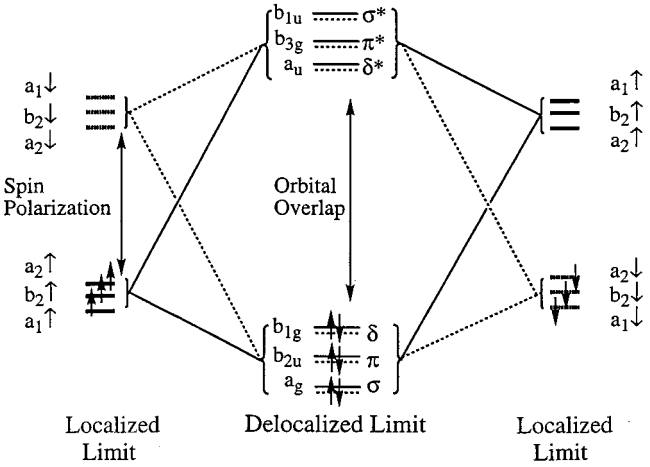

Figure 1. Representation of the broken-symmetry state of $\{d^3d^3\}$ edge-shared dimers in both localized and delocalized limits. Orbitals are labeled according to the representations of the C_{2v} point group in the localized limit and the D_{2h} point group in the delocalized limit. Spin polarization results in a splitting between the occupied and vacant single-ion orbitals in the localized limit whereas the splitting between bonding and antibonding molecular orbitals in the delocalized limit arises from direct metal−metal orbital overlap.

The calculated metal−metal separations for the heterobimetallic species are intermediate between those of homobimetallic complexes comprising the component metal ions. The short metal−metal separation of 2.76 Å calculated for $MoWCl_6(H_2PCH_2PH_2)_2$ is in good agreement with the known structures for $MoWCl_6(dmpm)_2$ and $MoWCl_6(dppm)_2$ and indicates that these complexes undergo strong metal−metal bonding consistent with the large antiferromagnetic exchange coupling constants of $J_{ab} = -1430$ cm^{-1} reported for both $MoWCl_6(dmpm)_2$ and $MoWCl_6(dppm)_2$.[5f] The much longer metal−metal distances of 3.32 and 3.06 Å calculated for $CrMoCl_6(H_2PCH_2PH_2)_2$ and $CrWCl_6(H_2PCH_2PH_2)_2$, respectively, are indicative of relatively weak antiferromagnetic coupling between the metal centers, although on the basis of bond lengths, the coupling is stronger than in the analogous dichromium system.

One notable difference between the structures of the $M_2Cl_{10}^{4-}$ and $M_2Cl_6(H_2PCH_2PH_2)_2$ complexes is that both the bridging MCl_{br} and terminal MCl_{eq} metal−chlorine bonds are shorter by as much as 0.20 Å in the phosphine-based complexes. From Mulliken population analyses, we find that the positive charge on the metal in $M_2Cl_6(H_2PCH_2PH_2)_2$ complexes is between 0.4 and 0.5 units lower than in $M_2Cl_{10}^{4-}$, presumably the result of the greater polarizability of the phosphine ligands. Furthermore, the negative charge on both the terminal and bridging chlorides, particularly the former, is smaller for the phosphine-based complexes, indicating that they are more electron donating in these species. A rationale for this increased donor character is that the phosphine ligands are behaving as weaker π donors, perhaps even π acceptors, and this forces the terminal and bridging chlorides to counter the loss of electron density on the metal through increased π donation.

(6) (a) Baerends, E. J.; Ellis D. E.; Ros, P. *Chem. Phys.* **1973**, *2*, 42. (b) Baerends, E. J.; Ros, P. *Int. J. Quantum Chem.* **1978**, *S12*, 169. (c) teVelde, G.; Baerends, E. J. *J. Comput. Phys.* **1992**, *99*, 84.
(7) Vosko, S. H.; Wilk, L.; Nusair, M. *Can. J. Phys.* **1980**, *58*, 1200.
(8) Versluis, L.; Ziegler, T. J. *Chem. Phys.* **1988**, *88*, 322.
(9) Ziegler, T. *Chem. Rev.* **1991**, *91*, 651.

Table 1. Optimized Structural Parameters for $M_2Cl_{10}^{4-}$, $M_2Cl_6(PH_3)_4$, and $M_2Cl_6(H_2PCH_2PH_2)_2$ (M = Cr, Mo, W) Complexes

	bond distances (Å)[a]					bond angles (deg)[a]				
complex	MM	MCl_{eq}	MCl_{br}	MCl_{ax}	MP	$Cl_{eq}MCl_{eq}$	$Cl_{br}MCl_{br}$	$Cl_{ax}MCl_{ax}$	PMP	$MCl_{br}M$
$Cr_2Cl_6(H_2PCH_2PH_2)_2$	3.43	2.23	2.37		2.40	95	87		175	93
$Mo_2Cl_6(H_2PCH_2PH_2)_2$	2.69	2.41	2.42		2.52	84	112		172	68
$W_2Cl_6(H_2PCH_2PH_2)_2$	2.76	2.44	2.47		2.56	84	112		173	68
$CrMoCl_6(H_2PCH_2PH_2)_2$	3.01	2.28	2.34		2.39	86	101		174	78
		2.37	2.45		2.52	88	101		180	
$CrWCl_6(H_2PCH_2PH_2)_2$	2.78	2.31	2.32		2.41	83	107		168	71
		2.42	2.46		2.58	88	100		177	
$MoWCl_6(H_2PCH_2PH_2)_2$	2.71	2.41	2.43		2.51	84			170	67
		2.43	2.45		2.57	84			173	
$Cr_2Cl_{10}^{4-}$	3.85	2.40	2.46	2.34		96	77	175		103
$Mo_2Cl_{10}^{4-}$	4.06	2.51	2.57	2.49		94	76	174		104
$W_2Cl_{10}^{4-}$	2.82	2.63	2.47	2.51		88	110	166		70
$CrMoCl_{10}^{4-}$	3.95	2.39	2.48	2.36		95		176		104
		2.52	2.55	2.49		94		174		
$CrWCl_{10}^{4-}$	3.99	2.39	2.48	2.36		96		177		104
		2.56	2.58	2.53		94		173		
$MoWCl_{10}^{4-}$	4.10	2.51	2.57	2.49		94		175		105
		2.54	2.60	2.53		94		174		
$Cr_2Cl_6(PH_3)_4$	3.51	2.25	2.36			97	84		171	96
$Mo_2Cl_6(PH_3)_4$	2.64	2.44	2.40			84	113		159	67
$W_2Cl_6(PH_3)_4$	2.69	2.46	2.46			84	114		159	67

[a] For heterobimetallic complexes, the first and second entries for each structural parameter correspond to the lighter and heavier metals, respectively.

Table 2. Experimental Structural Parameters for $M_2Cl_6(dmpm)_4$ and $M_2Cl_6(dppm)_2$ (M = Cr, Mo, W) Complexes

	bond distances (Å)[a]				bond angles (deg)[a]			
complex	MM	MCl_{eq}	MCl_{br}	MP	$Cl_{eq}MCl_{eq}$	$Cl_{br}MCl_{br}$	PMP	$MCl_{br}M$
$Cr_2Cl_6(dmpm)_2$	3.48	2.28	2.38	2.47	94	86	172	94
$Mo_2Cl_6(dmpm)_2$	2.74	2.43	2.39	2.55	85	110		70
$Mo_2Cl_6(dppm)_2$	2.79	2.40	2.40	2.59	85	109	174	71
$W_2Cl_6(dmpm)_2$	2.67	2.44	2.39	2.53	84	112		68
$W_2Cl_6(dppm)_2$	2.69	2.41	2.40	2.56	84	112		68
$MoWCl_6(dmpm)_2$	2.68	2.44	2.38	2.53	84	112	172	69
$MoWCl_6(dppm)_2$	2.72	2.41	2.40	2.58	84	111	173	69

[a] Because of crystallographic disorder, the structural parameter values for $MoWCl_6(dmpm)_2$ and $MoWCl_6(dppm)_2$ are averaged over both metal centers.

The homobimetallic decahalide complexes $M_2Cl_{10}^{4-}$ are calculated to have longer metal−metal separations than their phosphine-bridged analogues $M_2Cl_6(H_2PCH_2PH_2)_2$, this difference being as much as 1.3 Å in the case of the molybdenum complexes. It is tempting to attribute this difference solely to the geometric constraints of the phosphine bridge that clearly will limit the separation of the metal centers. However, the calculated metal−metal separations listed in Table 1 for the unbridged phosphine complexes $M_2Cl_6(PH_3)_4$ do not support this hypothesis. The fact that the calculated metal−metal separations for $M_2Cl_6(H_2PCH_2PH_2)_2$ and $M_2Cl_6(PH_3)_4$ complexes are almost identical implies that the shorter metal−metal separations in the former relative to the decahalide complexes arise purely from the replacement of the axial chlorides by phosphine donors and not as a result of any steric constraints imposed by the phosphine bridge structure. To rationalize this result and also to address periodic trends in metal−metal bonding, it is instructive to examine the potential energy curves for the three edge-shared systems $M_2Cl_{10}^{4-}$, $M_2Cl_6(PH_3)_4$, and $M_2Cl_6(H_2PCH_2PH_2)_2$. In this manner, it should be possible to monitor independently the effects of first replacing the axial chlorides with phosphine ligands and then introducing the methylene bridge unit.

Potential Energy Curves: General Features. As we have shown previously for $M_2Cl_9^{3-}$ and $M_2Cl_{10}^{4-}$ (M = Cr, Mo, W) complexes,[4] the analysis of the broken-symmetry potential energy curves in terms of the corresponding curves for the associated spin states of the dimer, where successive subsets (σ, π, and δ) of magnetic electrons are decoupled, provide a convenient means of monitoring the metal−metal interaction as the metal−metal distance changes. Irrespective of the extent of localization or delocalization of the magnetic orbitals, the broken-symmetry state in all three edge-shared systems can be described within C_{2v} symmetry by the configuration $(a_1\uparrow)^1(a_1\downarrow)^1(b_2\uparrow)^1(b_2\downarrow)^1(a_2\uparrow)^1(a_2\downarrow)^1(a_2\uparrow)^0(a_2\downarrow)^0(b_2\uparrow)^0(b_2\downarrow)^0(a_1\uparrow)^0(a_1\downarrow)^0$, where the σ, π, and δ subsets of electrons on opposite metal centers are antiferromagnetically coupled (see Figure 1). Depending on which subsets of electrons are involved in weak antiferromagnetic coupling (localized) and which are involved in strong metal−metal bonding (delocalized), four distinct descriptions of the broken-symmetry state are possible over a range of metal−metal distances corresponding to (a) all electrons delocalized, (b) $\sigma + \pi$ delocalized, δ localized, (c) σ delocalized, $\pi + \delta$ localized, and (d) all electrons localized. Where the overlap of a particular subset of magnetic orbitals is weak, the states corresponding to antiferromagnetic and ferromagnetic coupling of the electrons within the same subset of magnetic orbitals will lie close in energy. Thus, in relation to the four coupling modes (a)−(d) above are four "associated" spin states where the localized subsets of electrons are ferromagnetically coupled. The orbital configurations corresponding to each of these associated states are depicted in Chart 2 and are defined using the full D_{2h} dimer symmetry for the homobimetallic complexes since the magnetic electrons are found to be completely delocalized, even in the absence of symmetry elements connecting the two metal centers.

At large metal−metal separations where all the magnetic orbitals are localized, the broken-symmetry state corresponds

Chart 2

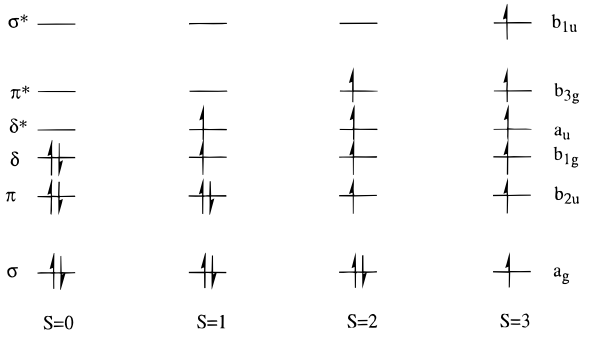

to weak antiferromagnetic coupling of the metal-based electrons, and therefore the $S = 3$ associated state, where σ, π, and δ subsets of electrons on opposite metal centers are aligned parallel, will lie closest in energy to the broken-symmetry state. At intermediate metal−metal separations, where the σ electrons are delocalized in a metal−metal σ bond but the π and δ subsets of electrons remain weakly coupled, the $S = 2$ associated state, corresponding to ferromagnetic coupling of the π and δ electrons, lies close in energy to the broken-symmetry state. At even shorter metal−metal separations where both the σ and π electrons are delocalized but the δ electrons remain weakly coupled, the $S = 1$ associated state lies closest in energy corresponding to ferromagnetic coupling of the δ electrons in isolation. Finally, at the shortest metal−metal separations, the σ, π, and δ subsets of electrons are all delocalized, and the $S = 0$ associated state, where all six metal-based electrons are paired up in the metal−metal σ, π, and δ bonding orbitals, converges with the broken-symmetry state.

$M_2Cl_{10}^{4-}$ and $M_2Cl_6(H_2PCH_2PH_2)_2$ Complexes. Potential energy curves for the broken-symmetry state and $S = 0-3$ associated states of the edge-shared decahalide $M_2Cl_{10}^{4-}$ and phosphine-bridged $M_2Cl_6(H_2PCH_2PH_2)_2$ complexes are shown in Figures 2 and 3, respectively. These curves highlight the dramatic difference in electronic structure and metal−metal bonding in the two edge-shared systems, particularly for the molybdenum and tungsten congeners. Qualitatively, the potential energy curves for $Cr_2Cl_6(H_2PCH_2PH_2)_2$ resemble those for $Cr_2Cl_{10}^{4-}$ in that the relative ordering of the associated states is the same, with $S = 0$ lying at highest energy and $S = 3$ at lowest energy. Thus, the global minimum in the broken-symmetry state occurs at a relatively long metal−metal separation, $r(Cr-Cr) = 3.43$ Å, corresponding to complete localization of all the metal-based electrons. However, although the two systems are similar, certain differences also exist. The mimima for the associated states span only 1 eV in $Cr_2Cl_6(H_2PCH_2PH_2)_2$, whereas in $Cr_2Cl_{10}^{4-}$ they are spread over 3.5 eV. For $Cr_2Cl_6(H_2PCH_2PH_2)_2$, the same minima also occur at metal−metal separations nearly 0.5 Å shorter than in $Cr_2Cl_{10}^{4-}$. These differences indicate that replacement of the axial chloride ligands by phosphine donors results in a reduction in the energetic barrier to metal−metal bond formation.

For the two heavier members of the series, the introduction of the phosphine bridge results in a dramatic change in the shape of the broken-symmetry potential energy curve compared to their decahalide counterparts. For both $Mo_2Cl_{10}^{4-}$ and $W_2Cl_{10}^{4-}$, the minima in the potential energy curves for the $S = 1$, $S = 2$, and $S = 3$ associated states are energetically close, leading to shallow double minima in the broken-symmetry potential energy curve over a relatively large range of r(M−M). This description of the broken-symmetry curve contrasts markedly with that observed in Figure 3 for $Mo_2Cl_6(H_2PCH_2PH_2)_2$ and $W_2Cl_6(H_2PCH_2PH_2)_2$. The potential energy curves for these two complexes are very similar, but instead of a relatively flat appearance over a wide range of r(M−M), the broken-symmetry curve is now distinctly steep-sided with a single, well-defined minimum in both cases. This abrupt change in shape can be attributed to a change in the energetic ordering of the associated states. In the decahalide complexes, the order is $S = 3 \leq S = 1 < S = 2 < S = 0$, with $S = 3$ lying lowest. In the phosphine-bridged complexes the ordering is $S = 1 < S = 2 < S = 0 < S = 3$, the $S = 3$ state undergoing a substantial destabilization relative to $S = 1$. The $S = 1$ state now lies lowest in both $Mo_2Cl_6(H_2PCH_2PH_2)_2$, and $W_2Cl_6(H_2PCH_2PH_2)_2$ and the global minimum in the broken-symmetry curve occurs at shorter metal−metal separations of 2.69 and 2.76 Å, respectively, corresponding to delocalization of both the σ and π subsets of metal-based electrons and thus a formal metal−metal double bond.

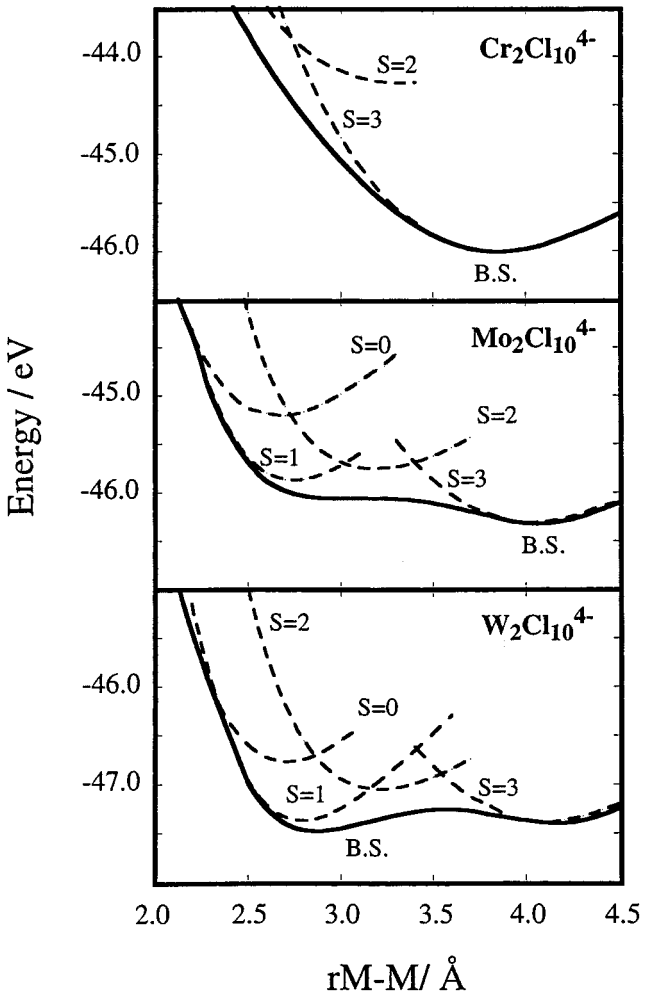

Figure 2. Potential energy curves for the broken-symmetry and $S = 0$, 1, 2, and 3 associated spin states in $\{d^3d^3\}$ $M_2Cl_{10}^{4-}$ (M = Cr, Mo, W) edge-shared dimers.

From Figures 2 and 3, it is apparent that the minimum in the $S = 0$ state, corresponding to complete delocalization of all metal-based electrons in a metal−metal triple bond, lies directly above $S = 1$ for all $M_2Cl_{10}^{4-}$ and $M_2Cl_6(H_2PCH_2PH_2)_2$ complexes. For the molybdenum and tungsten congeners, this reversed ordering persists down to quite short metal−metal separations, and only below 2.3 Å do the δ electrons finally delocalize. The reluctance of the δ electrons to delocalize is due to the well-established inversion of the δ and δ^* orbitals in edge-shared systems arising as a consequence of the destabilization of the δ orbital through interaction with a halide

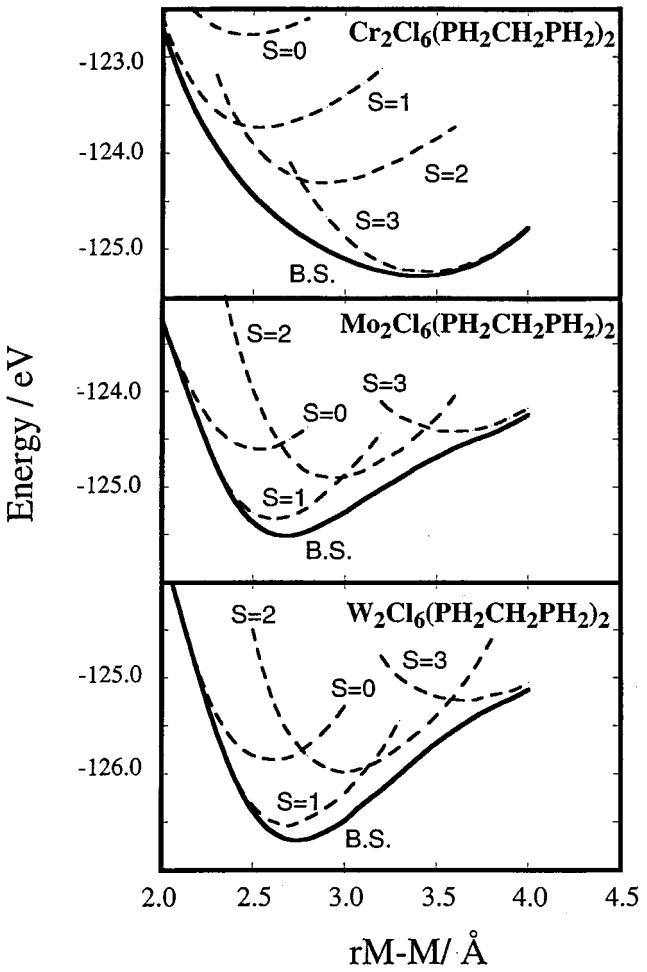

Figure 3. Potential energy curves for the broken-symmetry and $S = 0$, 1, 2, and 3 associated spin states in $\{d^3d^3\}$ $M_2Cl_6(H_2PCH_2PH_2)_2$ (M = Cr, Mo, W) edge-shared dimers.

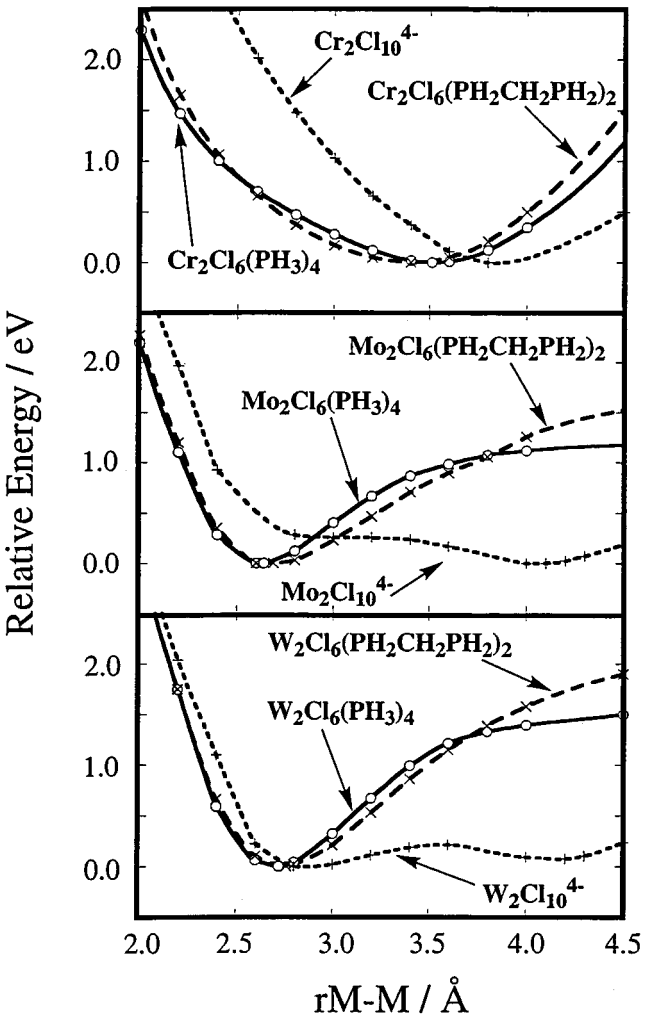

Figure 4. Comparison of the broken-symmetry potential energy curves for $\{d^3d^3\}$ $M_2Cl_{10}^{4-}$, $M_2Cl_6(PH_3)_4$, and $M_2Cl_6(H_2PCH_2PH_2)_2$ (M = Cr, Mo, W) edge-shared dimers.

bridge orbital of the same symmetry. Only where r(M−M) < 2.3 Å does the through space interaction dominate, and the δ orbital lies below δ^*. As a result of this inversion, the alternative $S = 0$ state, where both the metal-based δ electrons occupy the δ^* orbital, is more stable for r(M−M) > 2.3 Å.

The potential energy curves shown in Figures 2 and 3 are in line with the expected trend toward greater delocalization of the metal-based electrons in the heavier members of the triad. This is reflected not only in the overall shape of the broken-symmetry curve, but also in the energetic separation of the $S = 0$ and $S = 3$ associated states. In both $Cr_2Cl_{10}^{4-}$ and $Cr_2Cl_6(H_2PCH_2PH_2)_2$, this separation is large enough to prevent any change in the relative order of $S = 0$ and $S = 3$ states, even on replacement of the axial chloride ligands with phosphine donors, and consequently the electrons remain localized. However, for the molybdenum and tungsten congeners, the greater delocalization of the metal-based electrons results in an increasing stabilization of $S = 0$ relative to $S = 3$. For both $Mo_2Cl_{10}^{4-}$ and $W_2Cl_{10}^{4-}$, $S = 0$ lies above $S = 3$, but in $Mo_2Cl_6(H_2PCH_2PH_2)_2$ and $W_2Cl_6(H_2PCH_2PH_2)_2$, this ordering is reversed, indicating that metal−metal bonding is stronger in the phosphine-bridged systems, a fact consistent with the shorter metal−metal separations calculated for these complexes compared with their decahalide counterparts.

$M_2Cl_6(PH_3)_4$ Complexes. From Figures 2 and 3, it is apparent that the replacement of the axial chloride donors with the bridging phosphine ligands has a profound influence on the nature of the potential energy curves, resulting in a significant enhancement in metal−metal bonding. However, it is by no means clear whether this difference arises purely from the steric limitations imposed by the phosphine bridge structure or as a result of electronic effects due to the inherent differences between phosphine and chlorine donors. To address this problem, the broken-symmetry potential energy curves for the unbridged phosphine complexes $M_2Cl_6(PH_3)_4$ (M = Cr, Mo, W) have been generated. Apart from the connecting methylene bridge structure, these complexes are essentially identical to $M_2Cl_6(H_2PCH_2PH_2)_2$, and therefore any differences in the potential energy curves for these two systems can be attributed unambiguously to the geometric constraints of the bridging architecture. The broken-symmetry potential energy curves for $M_2Cl_6(PH_3)_4$ complexes are shown in Figure 4 along with those for the corresponding $M_2Cl_{10}^{4-}$ and $M_2Cl_6(H_2PCH_2PH_2)_2$ complexes. The most obvious feature emerging from a comparison of these curves is the close similarity of the broken-symmetry curves for $M_2Cl_6(PH_3)_4$ and $M_2Cl_6(H_2PCH_2PH_2)_2$ over the range 2.0 < r(M−M) < 3.8 Å. This similarity clearly indicates that the dramatic differences observed in the broken-symmetry curves for $M_2Cl_{10}^{4-}$ and $M_2Cl_6(H_2PCH_2PH_2)_2$, leading to overall shorter metal−metal separations and consequently stronger metal−metal bonding in the latter, can be directly attributed to electronic differences between chloride and phosphine donors rather than any geometric constraints imposed by the phospine bridge. For r(M−M) > 3.8 Å, however, the

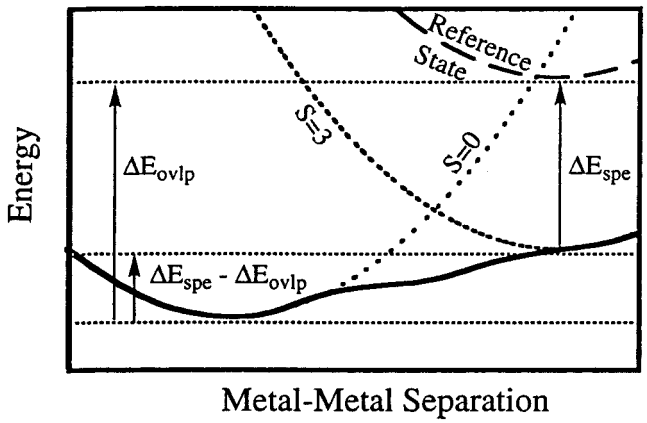

Figure 5. Schematic representation of the terms ΔE_{spe} and ΔE_{ovlp} in relation to the $S = 0$, S_{max}, and reference states of $\{d^3d^3\}$ edge-shared dimers.

constraining effect of the phosphine bridge structure is evident from the observed divergence of the broken-symmetry curves for the $M_2Cl_6(PH_3)_4$ and $M_2Cl_6(H_2PCH_2PH_2)_2$ complexes.

Electron Delocalization. From the above analysis, it is evident that the metal-based electrons are significantly more delocalized in both $M_2Cl_6(PH_3)_4$ and $M_2Cl_6(H_2PCH_2PH_2)_2$ complexes, resulting in stronger metal−metal bonding in these systems compared to $M_2Cl_{10}^{4-}$. To appreciate the underlying electronic properties of the metal ions which cause these differences and the resulting periodic trends in metal−metal bonding, it is desirable to obtain quantitative measures of the factors which affect the delocalization of the metal-based electrons in these systems. From earlier discussion, the extent of delocalization of the metal-based electrons is dictated by two terms, namely, the spin-polarization energy, favoring localization of the metal-based electrons, and the energy associated with orbital overlap, favoring delocalization. These two terms are in direct opposition, and consequently, the position of the localized/delocalized equilibrium will depend on their relative magnitudes. Similar qualitative arguments have been presented to rationalize the effects of different phosphine substituents on the metal−metal bonding in edge-shared $Mo_2Cl_6(PR_3)_4$ ($PR_3 = PEt_3$, PMe_2Ph) dimers.[5f,g]

As we have shown previously,[1c] the $S = 0$ associated state, corresponding to complete delocalization of the σ, π, and δ subsets of electrons in a metal−metal triple bond, has no spin-polarization contribution, whereas the $S = 3$ associated state, where the electrons on opposite metal centers are aligned parallel, has no orbital overlap contribution. The depth of the minima in the potential energy curves for the $S = 0$ and $S = 3$ states can therefore be equated with separate contributions from orbital overlap and spin polarization, respectively, as illustrated in Figure 5 (it should be noted that, as a result of the inversion of the δ and δ^* orbitals, the alternative $S = 0$ associated state, where the electrons occupy the δ^* orbital rather than δ, is the preferred $S = 0$ configuration in the following analysis). To obtain independent measures of these quantities, it is necessary to define an appropriate reference state where the contributions from both spin-polarization and orbital overlap terms are eliminated. Such a reference state corresponds to the configuration $(a_g\uparrow)^{0.5}(a_g\downarrow)^{0.5}(b_{2u}\uparrow)^{0.5}(b_{2u}\downarrow)^{0.5}(b_{1g}\uparrow)^{0.5}(b_{1g}\downarrow)^{0.5}(a_u\uparrow)^{0.5}(a_u\downarrow)^{0.5}(b_{3g}\uparrow)^{0.5}(b_{3g}\downarrow)^{0.5}(b_{1u}\uparrow)^{0.5}(b_{1u}\downarrow)^{0.5}$, where half a spin-up and half a spin-down electron is placed in each of the σ, π, and δ bonding and antibonding orbitals. The separation of the reference and $S = 0$ states therefore measures the energetic contribution of orbital overlap, denoted ΔE_{ovlp}, while the separation between the reference and $S = 3$ states is associated with that of spin polarization, ΔE_{spe}. The difference between these two terms, $\Delta E_{spe} - \Delta E_{ovlp}$, which is simply the energetic separation of the minima for the $S = 3$ and $S = 0$ states, quantifies the tendency of the metal-based electrons to delocalize and thus determines the position of the localization/delocalization equilibrium in each complex. The terms ΔE_{spe} and ΔE_{ovlp}, and their difference, $\Delta E_{spe} - \Delta E_{ovlp}$, are summarized in Table 3 for $M_2Cl_{10}^{4-}$ and $M_2Cl_6(H_2PCH_2PH_2)_2$ complexes examined in this study. The single-ion spin-polarization energies (SPE) for the relevant monomeric fragments MCl_6^{3-} and *trans*-$MCl_4(PH_3)_2^-$ occurring in these systems are also given for comparison. The latter were determined from the energy difference between restricted and unrestricted calculations corresponding to the single-ion configurations $[(t_{2g}\uparrow)^{1.5}(t_{2g}\downarrow)^{1.5}]$ and $[(t_{2g}\uparrow)^3(t_{2g}\downarrow)^0]$ in the case of octahedral MCl_6^{3-}, and $[(a_1\uparrow)^{0.5}(b_2\uparrow)^{0.5}(a_2\uparrow)^{0.5}(a_1\downarrow)^{0.5}(b_2\downarrow)^{0.5}(a_2\downarrow)^{0.5}]$ and $[(a_1\uparrow)^1(b_2\uparrow)^1(a_2\uparrow)^1(a_1\downarrow)^0(b_2\downarrow)^0(a_2\downarrow)^0]$ for the *trans*-$MCl_4(PH_3)_2$ fragment possessing C_{2v} symmetry.

Periodic Trends. The progressive reduction in the single-ion MCl_6^{3-} spin-polarization energies down the triad, with the most dramatic change occurring between the first and second transition series, has been noted previously[1c,4] and is simply a consequence of the increased radial dilation of the molybdenum 4d and tungsten 5d orbitals, which in turn reduces the average interelectronic repulsion. The replacement of the two axial chloride ligands with PH_3 produces a common reduction in the single-ion spin-polarization energy of approximately 0.3 eV relative to that of the hexachloride ions, a result of increased metal−ligand covalency which delocalizes spin density from the metal onto the phosphine ligands. In all three edge-shared systems, ΔE_{spe} for the dimer is very close to twice the relevant single-ion spin-polarization energy, implying that ΔE_{spe} is relatively insensitive to the bridging architecture. Down a triad but within the same edge-shared system, ΔE_{ovlp} is observed to increase, again a consequence of the increased dilation of the 4d and 5d orbitals. For the same metal ion, an increase in ΔE_{ovlp} between 0.9 and 1.1 eV is observed from $M_2Cl_{10}^{4-}$ to the phosphine-based system. The large increase in ΔE_{ovlp} implies an appreciable enhancement in metal−metal bonding occurs on exchanging the axial chlorides with phosphine, and presumably this arises from the increased dilation of the metal d orbitals due to the high covalency of the metal−phosphine bonds.

In both edge-shared systems, the tendency of the metal-based electrons to delocalize, as measured by the quantity $\Delta E_{spe} - \Delta E_{ovlp}$, is seen to progressively increase down the triad. Furthermore, within each edge-shared system, the overall trend toward greater delocalization in the complexes of the heavier metals is caused by approximately equal but opposite changes in ΔE_{spe} and ΔE_{ovlp}, as observed previously in our study of the face-shared $M_2Cl_9^{3-}$ (M = Cr, Mo, W) system.[1c] We note, however, that for the decachloride system, $\Delta E_{spe} - \Delta E_{ovlp}$ is still positive even for the tungsten complex, whereas in the $M_2Cl_6(H_2PCH_2PH_2)_2$ system, this quantity is negative for both the molybdenum and tungsten congeners. The lower values of $\Delta E_{spe} - \Delta E_{ovlp}$ obtained for the phosphine-based system thus confirm the greater delocalization and stronger metal−metal bonding in these complexes relative to the decachlorides. In all cases, the tendency toward greater delocalization is driven by a larger change in ΔE_{ovlp}, which, for the molybdenum and tungsten congeners, is at least double that of ΔE_{spe}. Consequently, for the second- and third-row metals, the increased tendency toward delocalized ground states in $M_2Cl_6(H_2PCH_2PH_2)_2$ relative to $M_2Cl_{10}^{4-}$ is dominated by changes in the metal−metal orbital overlap energy rather than spin polarization.

Table 3. Overlap and Spin Polarization Energies (eV) for $M_2Cl_{10}^{4-}$ and $M_2Cl_6(H_2PCH_2PH_2)_2$ (M = Cr, Mo, W) Complexes

complex	ΔE_{ovlp}	ΔE_{spe}	$\Delta E_{spe} - \Delta E_{ovlp}$	complex	single-ion SPE[a]
$Cr_2Cl_6(H_2PCH_2PH_2)_2$	1.328	2.971	+1.643	$CrCl_4(PH_3)_2^-$	1.52
$Mo_2Cl_6(H_2PCH_2PH_2)_2$	2.751	1.736	−1.015	$MoCl_4(PH_3)_2^-$	0.87
$W_2Cl_6(H_2PCH_2PH_2)_2$	2.967	1.568	−1.399	$WCl_4(PH_3)_2^-$	0.78
$CrMoCl_6(H_2PCH_2PH_2)_2$	1.978	2.360	+0.382		
$CrWCl_6(H_2PCH_2PH_2)_2$	2.089	2.279	+0.190		
$MoWCl_6(H_2PCH_2PH_2)_2$	2.859	1.656	−1.203		
$Cr_2Cl_{10}^{4-}$	0.430	3.626	+3.196	$CrCl_6^{3-}$	1.86
$Mo_2Cl_{10}^{4-}$	1.652	2.238	+0.586	$MoCl_6^{3-}$	1.14
$W_2Cl_{10}^{4-}$	1.903	2.037	+0.134	WCl_6^{3-}	1.03
$CrMoCl_{10}^{4-}$	0.949	2.931	+1.982		
$CrWCl_{10}^{4-}$	1.045	2.833	+1.788		
$MoWCl_{10}^{4-}$	1.775	2.136	+0.361		

[a] Single-ion SPE values are for MCl_6^{3-} and $MCl_4(PH_3)_2^-$ monomeric fragments.

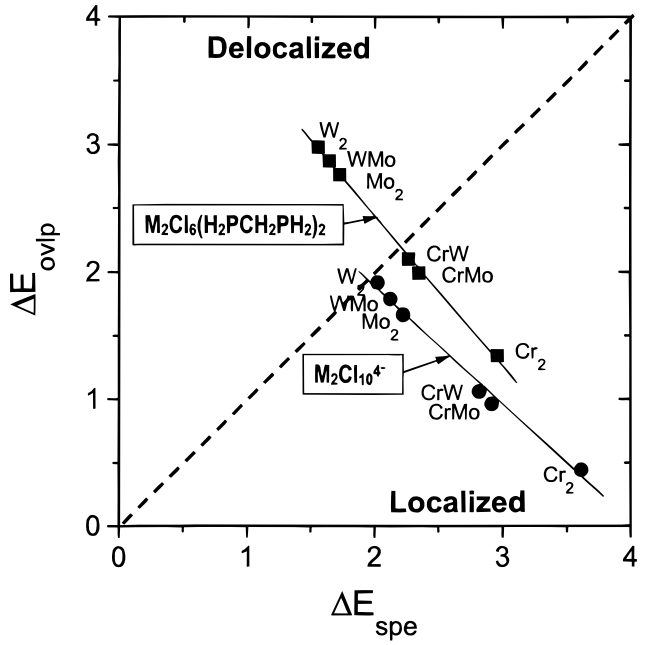

Figure 6. ΔE_{ovlp} versus ΔE_{spe} for homo- and heterobimetallic $\{d^3d^3\}$ $M_2Cl_{10}^{4-}$ and $M_2Cl_6(H_2PCH_2PH_2)_2$ (M = Cr, Mo, W) edge-shared dimers. The diagonal dashed line separates those systems which are delocalized ($\Delta E_{ovlp} > \Delta E_{spe}$) from those which are localized ($\Delta E_{ovlp} < \Delta E_{spe}$).

In the case of the heterobimetallic systems, Table 3 indicates that the ΔE_{spe} values are simply the sum of the component single-ion spin-polarization energies and the corresponding ΔE_{ovlp} values are approximately the average of those of the related homobimetallic systems. Consequently, the extent of delocalization of the metal-based electrons in heterobimetallic systems, as measured by $\Delta E_{spe} - \Delta E_{ovlp}$, is found to occur at intermediate positions, approximately midway between those of the homobimetallic complexes comprising the same metal ions.

The nature of the localized/delocalized equilibria can be best appreciated from Figure 6 where ΔE_{ovlp} is plotted against ΔE_{spe} for all complexes listed in Table 3. The fact that all the decachloride complexes are located in the lower triangle clearly demonstrates the more localized nature of the metal-based electrons in this system compared to $M_2Cl_6(H_2PCH_2PH_2)_2$. The presence of the axially coordinated phosphine ligands thus affords greater delocalization of the metal spin density onto the ligands, thereby reducing the spin-polarization energy while enhancing metal−metal orbital overlap. For both edge-shared systems, a strong linear dependence between ΔE_{spe} and ΔE_{ovlp} is observed. Consequently, since ΔE_{spe} for the dimer is essentially the sum of the single-ion spin polarization energies, the localization/delocalization equilibria, and therefore the extent of metal−metal bonding in these systems, can be predicted simply on the basis of the component single-ion spin-polarization energies.

Magnetic Properties. Using spin-projection techniques, Noodleman[2] has shown that when the magnetic interaction is weak, the exchange coupling constant J_{ab} is given by

$$-J_{ab} = [E(S_{max}) - E_B]/{S_{max}}^2 \quad (1)$$

where $E(S_{max})$ and E_B are the energies of the ferromagnetic state, S_{max}, and broken-symmetry state, respectively. Since this expression is only valid in the limit of weak coupling, it is necessary to distinguish which subset(s) of electrons are weakly coupled and which are involved in strong metal−metal bonding as this will necessarily determine which ferromagnetic state S_{max} is applicable. Our previous study[1b] of the face-shared $M_2Cl_9^{3-}$ (M = Cr, Mo, W) system revealed that an inappropriate value of S_{max} can lead to a significant overestimation of J_{ab}. Consequently, if there is any doubt about which value of S_{max} is applicable, the better choice will be the value of S_{max} that yields the lowest value of J_{ab}.

The observed and calculated values of J_{ab} for $M_2Cl_6(H_2PCH_2PH_2)_2$ complexes, along with the relevant values for S_{max} used in calculating J_{ab}, are summarized in Table 4. In addition, both the uncorrected and covalency-corrected spin densities on each metal in the broken-symmetry state are given in Table 4, the latter taking into account the reduction in spin density due to metal−ligand covalency effects. The covalency-corrected spin density can be equated with the number of unpaired electrons on each metal involved in the coupling and therefore provides an indication of the value of S_{max} in eq 1.

Experimentally, $Cr_2Cl_6(dmpm)_2$ exhibits very weak antiferromagnetic coupling with a reported $-J_{ab}$ of less than 2 cm^{-1}.[5e] This, combined with the long metal−metal separation of 3.48 Å, suggests that σ, π, and δ subsets of magnetic electrons are weakly coupled. This description of the coupling is supported by the high percent localization of the magnetic orbitals in the broken-symmetry state shown in Figure 7 and also the corrected spin density of 2.96. Almost all the reduction in the uncorrected spin density from 3.0 can be attributed to metal−ligand covalency as the spin density for the monomeric fragment $CrCl_4(PH_3)_2^-$ is calculated to be 2.88. From the potential energy curves for $Cr_2Cl_6(H_2PCH_2PH_2)_2$ shown in Figure 3, the $S = 3$ state is observed to converge with the global minimum in the broken-symmetry curve at approximately 3.4 Å. Therefore, the appropriate ferromagnetic state required in eq 1 corresponds to

Table 4. Magnetic Data for $M_2Cl_6(H_2PCH_2PH_2)_2$ (M = Cr, Mo, W) Complexes

complex	observed J_{ab} (cm^{-1}) dmpm	observed J_{ab} (cm^{-1}) dppm	calculated J_{ab} (cm^{-1})[a]	uncorrected dimer spin density S_a:S_b	covalency-corrected dimer spin density[b] S_a:S_b
$Cr_2Cl_6(H_2PCH_2PH_2)_2$	−2		−26 (S_{max} = 3)	2.84:2.84	2.96:2.96
$Mo_2Cl_6(H_2PCH_2PH_2)_2$	−755	−730	−1087 (S_{max} = 1) −1180 (S_{max} = 2)	0.98:0.98	1.20:1.20
$W_2Cl_6(H_2PCH_2PH_2)_2$	−565	−615	−989 (S_{max} = 1) −1392 (S_{max} = 2)	0.88:0.88	1.11:1.11
$CrMoCl_6(H_2PCH_2PH_2)_2$			−90 (S_{max} = 3) −690 (S_{max} = 2)	2.54:2.11	2.65:2.57
$CrWCl_6(H_2PCH_2PH_2)_2$			−152 (S_{max} = 3) −577 (S_{max} = 2)	2.18:1.72	2.27:2.18
$MoWCl_6(H_2PCH_2PH_2)_2$	−715	−715	−1057 (S_{max} = 1) −1284 (S_{max} = 2)	0.93:0.89	1.13:1.13

[a] The value of S_{max} used in eq 1 to calculate J_{ab} is given in parentheses. [b] Covalency correction to dimer spin density given by 3.0/(monomer spin density) where the monomer spin density corresponds to the calculated values of 2.88 (Cr), 2.46 (Mo), and 2.37 (W) for the relevant $MCl_4(PH_3)_2^-$ fragment.

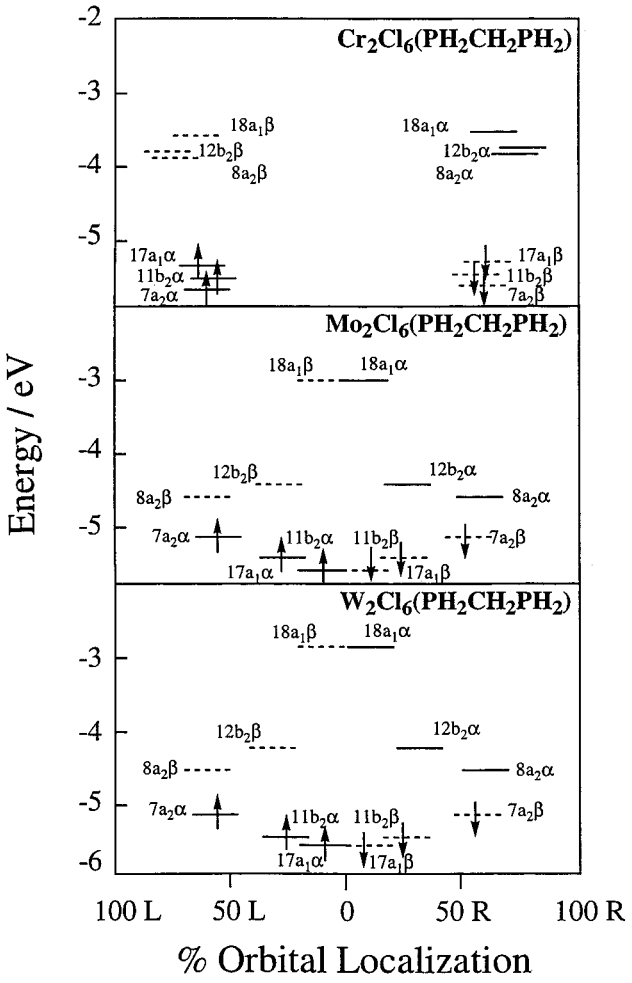

Figure 7. Energies of the broken-symmetry spin-up (α) and spin-down (β) magnetic orbitals for $\{d^3d^3\}$ $M_2Cl_6(H_2PCH_2PH_2)_2$ (M = Cr, Mo, W) edge-shared dimers showing their percent localization on either the left or right metal center of the dimer.

S_{max} = 3, yielding a value of $-J_{ab}$ = 26 cm^{-1} consistent with the weak antiferromagnetic coupling observed for $Cr_2Cl_6(dmpm)_2$.

The data in Table 4 reveal that $Mo_2Cl_6(L-L)_2$, $W_2Cl_6(L-L)_2$, and $MoWCl_6(L-L)_2$ (L−L = dmpm, dppm) all display very strong antiferromagnetic coupling with the reported $-J_{ab}$ values ranging from 565 to 755 cm^{-1}, depending on the phosphine substituent and whether J_{ab} was determined from bulk magnetic susceptibility measurements or $^{31}P\{^1H\}$ NMR spectra.[5f] The reported metal−metal distances of 2.67 and 2.69 Å for $W_2Cl_6(dmpm)_2$ and $W_2Cl_6(dppm)_2$ are close to the global minimum in the broken-symmetry curve for $W_2Cl_6(H_2PCH_2PH_2)_2$. At these distances the S = 1 state lies closest to the broken-symmetry curve, and therefore the broken-symmetry state is best described in terms of delocalized σ and π electrons but weakly coupled δ electrons. However, the covalency-corrected spin density of 1.11 indicates that the π electrons are not completely delocalized, and this agrees with the 25% localization of the π magnetic orbitals ($11b_2\alpha$, $11b_2\beta$) in Figure 7. Consequently, although the observed antiferromagnetic behavior for $W_2Cl_6(dmpm)_2$ and $W_2Cl_6(dppm)_2$ can be largely attributed to coupling of the δ electrons, some contribution from the π electrons must be invoked. Given that the antiferromagnetism is dominated by coupling of the δ electrons, the appropriate ferromagnetic state is S_{max} = 1, resulting in $-J_{ab}$ = 989 cm^{-1}. If the π subsets of electrons are assumed to be fully involved in the exchange coupling, then S_{max} is 2 and a value of $-J_{ab}$ = 1392 cm^{-1} is now calculated in much poorer agreement with the experimental data.

On the basis of the similar potential energy curves for $Mo_2Cl_6(H_2PCH_2PH_2)_2$ and $W_2Cl_6(H_2PCH_2PH_2)_2$, it is reasonable to assume that the magnetic coupling in the molybdenum complexes is comparable to that in the tungsten analogues and therefore determined predominantly by coupling of the δ electrons. However, since the reported metal−metal distances of 2.74 and 2.79 Å for $Mo_2Cl_6(dmpm)_2$ and $Mo_2Cl_6(dppm)_2$ are both longer than the optimized value of 2.69 Å for $Mo_2Cl_6(H_2PCH_2PH_2)_2$, and the energetic separation of the S = 1 and S = 2 curves is smaller relative to that of $W_2Cl_6(H_2PCH_2PH_2)_2$, it is possible that the π electrons make a greater contribution toward the exchange coupling in the molybdenum complexes. From Table 4 we note that the lowest value of J_{ab} is obtained for S_{max} = 1, but the value for S_{max} = 2, where the π electrons are explicitly included, is only 93 cm^{-1} higher. At 2.79 Å, however, corresponding to the metal−metal distance for $Mo_2Cl_6(dppm)_2$, the covalency-corrected spin density is nearly 1.4, the π magnetic orbitals are almost 50% localized on either molybdenum center, and J_{ab} is smallest when S_{max} = 2. All of these factors indicate that, at ∼2.8 Å, the π electrons are moderately involved in the exchange coupling. Further evidence of their involvement is apparent from Figure 8 where the dependence of J_{ab} on both r(M−M) and S_{max} is shown for $Mo_2Cl_6(H_2PCH_2PH_2)_2$. For $Mo_2Cl_6(dmpm)_2$ and $Mo_2Cl_6(dppm)_2$, r(M−M) lies very near the crossover region between S_{max} = 1 and S_{max} = 2. As a result, the calculated J_{ab} values are very similar for S_{max} = 1 and 2, and therefore both δ and π subsets of electrons are involved in the exchange coupling. Our

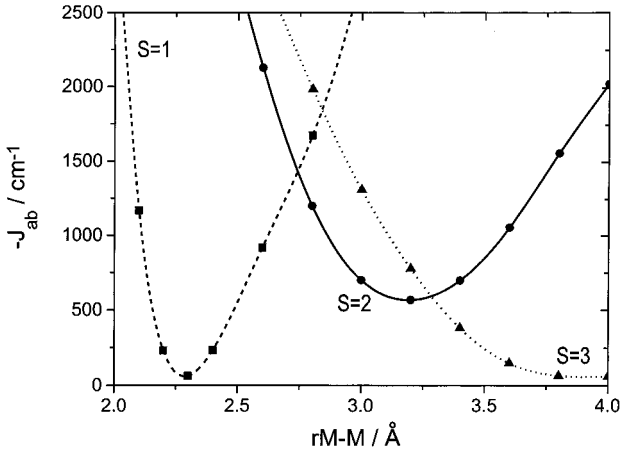

Figure 8. Dependence of $-J_{ab}$ on metal−metal separation and S_{max} in $Mo_2Cl_6(H_2PCH_2PH_2)_2$. The $-J_{ab}$ values are calculated using eq 1 (see the text) with $S_{max} = 1$, 2, and 3.

findings basically parallel those of a recent CASSCF study of the same model complex where the metal−metal separation was fixed at 2.79 Å.[11]

The J_{ab} values, spin densities, and metal−metal distances calculated for the heterobimetallic species lie between those of the homobimetallic analogues, suggesting that the electronic and magnetic properties of these systems are simply the average of those of the component metals. This theoretical result is supported by the experimental data in that the reported values of J_{ab} and r(M−M) for $MoWCl_6(dmpm)_2$ and $MoWCl_6(dppm)_2$ lie between those of the corresponding dimolybdenum and ditungsten complexes. It is interesting to note that, once the covalency correction is applied, the spin densities on both metals in the heterobimetallic systems are very similar. From Table 3, the spin densities of 2.65 (Cr) and 2.57 (Mo) in $CrMoCl_6(H_2PCH_2PH_2)_2$ indicate that the magnetic electrons are more or less localized on the metal centers, and therefore $S_{max} = 3$ is applicable. The calculated value of $-J_{ab} = 90$ cm^{-1} is an order of magnitude smaller than for $Mo_2Cl_6(H_2PCH_2PH_2)_2$ but significantly larger than the calculated value of 26 cm^{-1} for the chromium analogue, reflecting the intermediate nature of the coupling in this complex. The substantially larger $-J_{ab}$ value of 690 cm^{-1} obtained when $S_{max} = 2$ justifies the use of $S_{max} = 3$ in calculating J_{ab}. In the case of $CrWCl_6(H_2PCH_2PH_2)_2$, the spin densities of 2.27 (Cr) and 2.18 (W) suggest that partial delocalization of the σ electrons has occurred, consistent with the reduced metal−metal separation and larger J_{ab} values compared to those of $CrMoCl_6(H_2PCH_2PH_2)_2$. Since the smallest J_{ab} is calculated for $S_{max} = 3$, this system can still be regarded as relatively weakly coupled. Finally, from the spin densities of 1.13 for both Mo and W in $MoWCl_6(H_2PCH_2PH_2)_2$, substantial delocalization of the metal-based σ and π subsets of electrons has occurred. The smallest J_{ab} value of 1057 cm^{-1} is calculated using $S_{max} = 1$, and therefore an arrangement similar to that of $W_2Cl_6(H_2PCH_2PH_2)_2$ exists where the δ subset of electrons are mainly involved in the coupling.

Finally, other workers have suggested that the singlet−triplet gap in the molybdenum complexes is relatively insensitive to the metal−metal separation.[11] The rationale behind this conclusion is that the coupling of the δ electrons is not determined from direct metal−metal orbital overlap but from superexchange interactions involving the halide bridge. However, the magnetic data for the phosphine-bridged dimolybdenum systems span a rather limited range of metal−metal distances, between 2.74 and 2.79 Å, which fall very close to the crossover region between the J_{ab} curves based on $S_{max} = 1$ and $S_{max} = 2$. From Figure 8 we observe that $-J_{ab}$ varies between 600 and 700 cm^{-1} over this range of r(M−M) (assuming ∼50% overestimation of J_{ab} by DFT), and this agrees rather well with the reported $-J_{ab}$ values between 545 and 755 cm^{-1}. From Figure 8, the limited range of $-J_{ab}$ can be attributed, at least in part, to the varying contribution of the π electrons to the exchange coupling. Below 2.75 Å, only the δ subset are involved, whereas above 2.75 Å, both δ and π electrons must be included. Outside the narrow range of r(M−M) found for these complexes, $-J_{ab}$ is clearly quite sensitive to the metal−metal separation. In fact, below 2.75 Å, $-J_{ab}$ is predicted to decrease from nearly 1500 cm^{-1} to as low as 50 cm^{-1} at around 2.3 Å. This reduction can be attributed to the onset of direct metal−metal δ orbital overlap as r(M−M) decreases, which, in the vicinity of 2.3 Å, results in the δ and δ^* orbitals being approximately degenerate.

Conclusion

Density functional theory has been successfully used to generate potential energy curves for the broken-symmetry and $S = 0-3$ associated states to investigate the electronic structures, geometries, and periodic trends in metal−metal bonding in the homo- and heterobimetallic d^3d^3 edge-shared systems $M_2Cl_{10}^{4-}$, $M_2Cl_6(PH_3)_4$, and $M_2Cl_6(H_2PCH_2PH_2)_2$ (M = Cr, Mo, W). Significantly, the much shorter metal−metal distances found for $M_2Cl_6(H_2PCH_2PH_2)_2$ complexes relative to $M_2Cl_{10}^{4-}$ have been shown to arise solely from electronic differences between chlorine and phosphine donors and not as a result of any structural constraints imposed by the phosphine bridge. The inversion of the δ and δ^* orbitals in $Mo_2Cl_6(H_2PCH_2PH_2)_2$ and $W_2Cl_6(H_2PCH_2PH_2)_2$ results in these complexes possessing metal−metal double bonds rather than triple bonds expected for d^3d^3 dimers. The analysis of the broken-symmetry potential energy curves in terms of the energetic contributions of orbital overlap (ΔE_{ovlp}) favoring delocalization and spin polarization (ΔE_{spe}) favoring localization has enabled the periodic trends in metal−metal bonding in these systems to be rationalized. Importantly, replacement of the axial chlorides with phosphine donors leads to a uniform reduction in ΔE_{spe} and an increase in ΔE_{ovlp}, both factors favoring stronger metal−metal bonding in the phosphine-based complexes. The antiferromagnetism of $M_2Cl_6(H_2PCH_2PH_2)_2$ (M = Mo, W) and $MoWCl_6(H_2PCH_2PH_2)_2$ has been found to be mainly due to coupling of the δ electrons with a partial contribution from the π electrons, particularly for the dimolybdenum species. The similar J_{ab} values reported for $M_2Cl_6(P-P)_2$ (M = Mo, W; P−P = dmpm, dppm) arise from the restricted range of metal−metal distances in these complexes, which fall within the crossover region associated with coupling of both the δ and π electrons.

Acknowledgment. The Australian Research Council is gratefully acknowledged for financial support and the Engineering and Physical Sciences Research Council (U.K.) for an overseas scholarship to T.L.

IC9905042

(10) Shaik, S.; Hoffmann, R.; Fisel, C. R.; Summerville, R. H. *J. Am. Chem. Soc.* **1980**, *102*, 4555.
(11) Cotton, F. A.; Feng, X. *Int. J. Quantum Chem.* **1996**, *58*, 671.